Int J Clin Exp Med 2017;10(2):2450-2459
www.ijcem.com /ISSN:1940-5901/IJCEM0040448

Original Article

Comparison among the imaging characteristics of the intravitreous wooden foreign body in rabbits

Baohong Wen[1], Jingliang Cheng[1], Huixia Zhang[1], Yong Zhang[1], Xiaonan Zhang[1], Chenyu Yan[1], Fengguang Zhang[2]

[1]*Department of MRI, The First Affiliated Hospital of Zhengzhou University, Zhengzhou, P. R. China;* [2]*Henan Tumor Hospital, Zhengzhou, P. R. China*

Received September 22, 2016; Accepted November 8, 2016; Epub February 15, 2017; Published February 28, 2017

Abstract: *Objective:* The intraocular foreign bodies (IOFBs) belong to the special ocular trauma. Diagnostic values (ultrasonography, CT/computed tomography and MRI/magnetic resonance imaging) of different imaging technologies for IOFBs in rabbit vitreous body were evaluated for clinical diagnosis. *Methods:* A total of 240 healthy rabbits were involved, 192 receiving the wooden IOFBs (f = 0.2 mm; different in lengths, materials and moisture states) implantation in the right vitreous. Imageological diagnosis was conducted 2 h, 2 weeks and 4 weeks after the surgery with the characteristics recorded and compared. Subsequently, the right eyebulb was extracted for pathological examination. *Results:* The detected IOFBs were punctate or linear low signals on MRI and showed strong echo of the light spot on sonogram. For 192 IOFBs, the detection rates were 49.5% and 71.4% for MRI and ultrasonography, respectively, with the minimum detectable length of 0.5 mm. The detection rates increased with the length. The detection rates of ultrasonography were significantly higher than those of MRI towards dry pine and China rose ($P<0.05$). Length was the major factor affecting the MRI detection rates, while the ultrasonography was unaffected by the length, material and moisture state. Detected diameters by MRI (0.227±0.045 mm) and the ultrasonography (0.250±0.050 mm) were extremely different from the actual diameter ($P<0.001$). Complication detection rates of IOFBs (Length = 2 mm) at 2 h, 2 w, and 4 w after the implantation among MRI, CT and ultrasonography differed insignificantly. *Conclusion:* MRI and ultrasonography were effective in diagnosing the IOFBs in rabbit ocular.

Keywords: Intraocular foreign bodies, vitreous body, magnetic resonance imaging, computer tomography, ultrasonography

Introduction

Ocular trauma is one common ophthalmic emergency inducing changes of optical anatomical structure and function, or even blinding [1-3]. Intraocular foreign bodies (IOFBs) are particularly serious in the ocular trauma, which usually happen to people of any age, esp. young adults and children at home or working place. IOFBs cause mechanical damages and the microbic infection during the retention inside the eyebulb or the orbital cavity [4]. Several complications could be generated due to the IOFBs stimulation to the ocular tissue. IOFBs are often accompanied with ocular perforating injuries and the retina/optic nerve injuries (e.g. sympathetic ophthalmia) impairing the bilateral visual function. For IOFBs inside the vitreous body, the inflammation will lead to the proliferative vitreoretinapathy and tractional detachment of retina, and the irreversible changes (e.g. blindness) eventually. Hence it's crucial for patients to remove the IOFBs timely and recover the visual function.

Mostly, IOFBs are caused by the firewood injury, branch puncture and blast injury, etc., inducing major ocular damages and inflammatory infections though infrequent. When entering the eyesocket under high speed, the IOFBs leaves negligible surface wound and heals fast, retarding patients from timely treatment [5, 6]. Wooden IOFBs are easily fractured due to the high brittleness and no broken ends can be detected, consequently causing misdiagnosis and missed diagnosis. Accurate and efficient detection is essential to the effective treatment and improvement of postoperative visual function.

With the development of imaging technology, ultrasonography (US), computed tomography (CT) and magnetic resonance imaging (MRI) have been extensively applied in the field of ophthalmology. The ultrasonography detection is unaffected by the IOFBs nature, realizing the real-time dynamic observation of ocular wall, lens, vitreous and the surrounding tissue structure. This technology is advantageous to the IOFBs location, but unclearly reveals those at the anterior segment and unfit for open wounds [7]. With high density resolution, CT distinctly illustrates the high-density IOFBs and reveals the positional information through three-dimensional reconstruction. But it's inappropriate for the detection of the low-density IOFBs and the induced complications [8-10]. Characterized by the high soft tissue resolution, MRI is sensitive to the non-magnetic low-density IOFBs, and presents the complications. But it's confined to the non-metallics, which can cause the movement of metals [11]. MRI has shown more remarkable advantages in optical traumas than CT, esp. in the imaging resolution of soft tissue (e.g. the optic nerve, optic chiasma and orbital contents) and in the characterization of intraocular non-magnetic foreign bodies (e.g. the wooden IOFBs and plastics) [12, 13]. It has been reported that MRI can investigate the damage of blood-retinal barrier and the retinal oxygenation reaction, which would become one of the main method in evaluating the retinal function [14]. In addition, MRI is suited for the assessment of vascular damage, providing rational basis for the clinical removal of foreign body [15]. The ultrasonography, CT and MRI can complement each other with their respective advantages in the diagnosis of IOFBs for improving the accuracy of location and detection and reducing the complications.

Based on the previous research, the paper was designed to optimize the parameters and utilize the ultrasonography, CT and MRI in the diagnosis of wooden IOFBs inside the rabbit vitreous. Through animal experiments, the imageological characteristics of wooden IOFBs (different in length, material and moisture states) were determined and compared for benefiting the clinicians to select effective methods in the diagnosis of IOFBs.

Materials and methods

Animals and wooden IOFBs

A total of 240 healthy Japanese rabbits (male/female; 2.0-2.5 Kg in weight; normal binocular vision) were obtained (Henan Kangda Laboratory Animal Co., Ltd., Zhengzhou, China).

Xylem parts of poplar (*Salicaceae*, Timber), paulownia (*Sterculiaceae*, Timber), pine (*Pinaceae*, Timber) and China rose (*Rosaceae*, Shrub) were selected for the implantation and gauged by the vernier caliper to be trimmed into cylinders (f = 0.2 mm) with different lengths (0.2 mm, 0.5 mm, 1.0 mm, and 2.0 mm, respectively). Xylems from fresh branches were defined as wet IOFBs, while those insolated for one month were recognized as dry IOFBs.

192 Animals were randomly selected and divided into four groups according to the lengths (48 rabbits per group), each of which was subgrouped by the materials (12 rabbits per subgroup). And then each subgroup was further divided by the moisture states (6 rabbits per experimental group). Other 48 rabbits were randomly divided into three groups for reference.

Animal models

Fasting and water-deprivation of experimental animals were performed 8 h before the implantation. Adequate amount of chloral hydrate (10%, 0.3 g/kg) was applied for transperitoneal induction of general anesthesia. Animals were maintained left lateral position and settled on the experiment table after anesthesia. The conjunctival layer (the avascular area), 3 mm above the limbus cornea of right eye, was cut off by sterile eye scissors. Sclera was fully exposed and then punctured with 1 mL sterile syringe. Wooden IOFBs were slowly lowered into the right vitreous with ophthalmic forceps. And the puncture site was sewed up with 8-0 absorbable sutures. Ofloxacin ointment was applied onto the injured right eye. Animals implanted with IOFBs (Length = 2 mm) were examined by the ultrasonography, CT and MRI, respectively, 2 h after the puncture. Preliminary tests indicated that CT could not detect wooden IOFBs (f = 0.2 mm) with length of 3 mm. Then rabbits in experimental groups implanted with wooden IOFBs with length of 1 mm, 0.5 mm and 0.2 mm were not diagnosed by CT. After the imageological inspection, two rabbits were randomly selected for immediate ocular enucleation and pathological examination. Remnant four rabbits in each experimental group were fed 2 weeks and then performed the same imageological examination. Two rabbits were randomly selected for ocular enucleation and subsequent pathological examination. And the remaining two rabbits in each sub-subgroup were fed for another 2 weeks (4 weeks after the surgery) and treated with the above examination procedure. Right vitreous of rabbits in the reference groups were traumatic for the similar puncture without foreign body implanted to exclude the pathological change caused by operative wound. Then ocular enucleation and pathological examination were conducted within the intervals in the experimental groups (2 h, 2 weeks and 4 weeks after the surgery, respectively). Daily chloramphenicol eye drops were regularly applied on the surgical eye during the dynamic observation of experimental animals.

MRI examination

All experiments were conducted on a Siemens 3.0 T Verio Scanner System. Head of experimental rabbit was centered into the dedicated coil (Shanghai Chenguang Medical Instrument Co., LTD.) in prone position to keep gaze downwards. Three-dimensional positioning images of the transverse plane, sagittal plane and coronal plane were obtained. Then axial scanning, oblique sagittal scanning and coronal scanning were conducted on the whole eye socket successively. Baseline of transverse scanning was perpendicular to the hard palate, while those of oblique sagittal scanning and coronal scanning were parallel to the optic nerve and the hard palate, respectively. T_1 weighted imaging (T_1WI) and T_2 weighted imaging (T_2WI) scanning sequence were selected in this paper.

Scanning parameters of T_1WI were as follows: TR/TE = 604.0 ms/13.0 ms, thickness = 1 mm, spatial resolution = 0.4 mm×0.4 mm×1.0 mm and field of view (FOV) = 10 cm×10 cm. Scanning parameters of T_2WI involved: TR/TE = 4260.0 ms/73.0 ms, thickness = 1 mm, spatial resolution = 0.3 mm×0.3 mm×1.0 mm and FOV = 10 cm×10 cm. For PDWI, the scanning parameters were TR/TE = 2500.0 ms/12.0 ms, thickness = 1 mm, spatial resolution = 0.4 mm×0.4 mm×1.0 mm and FOV = 10 cm×10 cm.

Original data and images were all sent to the Siemens 3.0 T Syngo post-processing workstation to record the number of detected foreign bodies and complication cases and then the diameters were calculated.

CT examination

CT examination was conducted by the High-definition Discovery CT750HD (GE Healthcare). The scanning parameters and reconstruction methods were as followed: tube voltage = 80 Kv, tube current = 200 As, speed = 0.8 sec/rev, pitch = 0.984:1, slice thickness = 1.25 mm, intra-layer spacing = 1.25 mm. Original data and reconstruction images of all experimental animals were transferred to the Advanced Workstation (AW 4.4). The spectrum scanning was chosen.

Transverse scan in bottom-up direction was first selected with the same baseline as the MRI. Experimental animals were settled in prone position with eyes straight forward. The sagittal and coronal reconstruction could be performed when necessary. Without the blood supply, IOFBs were uninvestigated by the enhancement scanning. The number and density of IOFBs, the number of complication cased and the CT value were recorded and the diameter was observed.

Ultrasonography examination

The login S6 color doppler ultrasonography and high-frequency linear array probe (7.0 MHz) (GE Healthcare) was adopted. Rabbits were settled in supine position with eyelids closed. The eyelid direct contact method was used: coupling agent was applied on the surface of the eyelids with binocular contrast adopted. The ultrasonic probe contacts the eyelids gently and avoids pressing the eyebulb, rotating from different directions to illustrate the cross-sectional images comprehensively. When exploring the IOFBs, the gain was adjusted to observe changes of lesions echo. With optimum image selected, the position was immobilized to measure the size and the number of detectable IOFBs. Then the echo intensity and relationship between IOFBs and surrounding tissue were observed besides the secondary lesions, e.g. the lens turbidity, vitreous hemorrhage, retinal detachment, and vitreous opacity.

Pathological examination

Experimental animals were executed according to the designed intervals and right eyeblub was extracted to conduct the pathological examination. The stationary liquid was prepared with the anhydrous alcohol, distilled

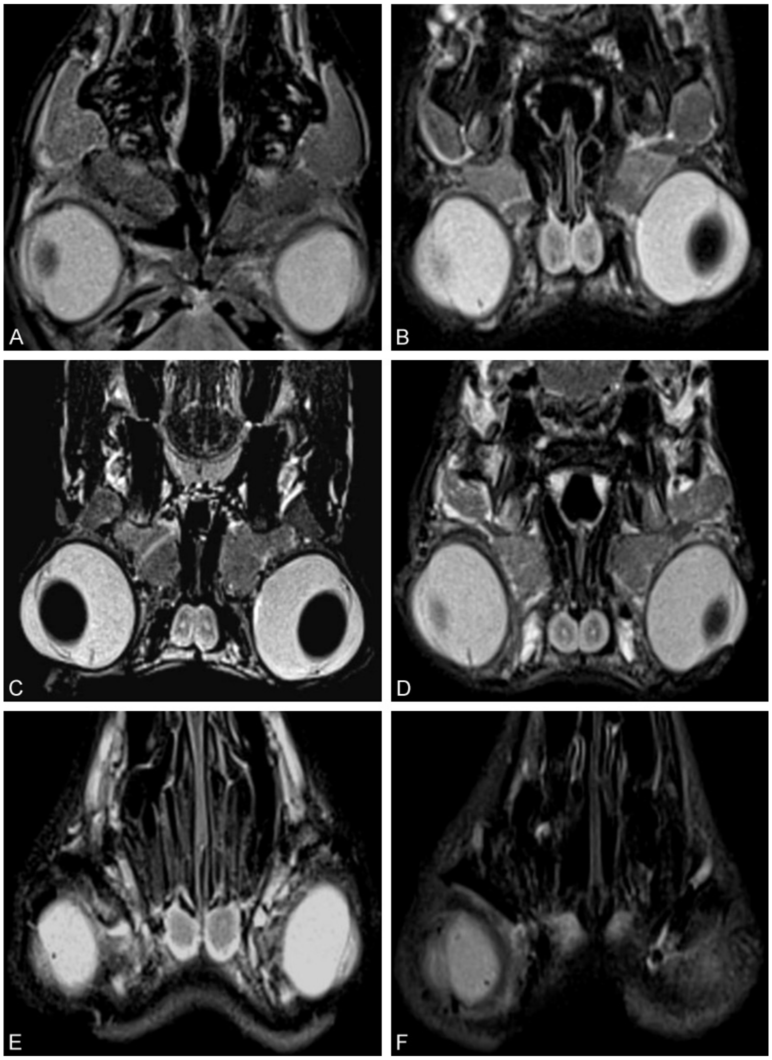

Figure 1. The characteristics of wooden IOFBs implanted in the rabbit right vitreous on typical transverse MRI (T_2WI) imaging. In (A) dry poplar (Length = 1 mm) presented as punctate or linear low signal after implanted for 2 h. In (B) wet paulownia (Length = 2 mm) presented as punctate or linear low signal after implanted for 2 h. In (C) dry pine (Length = 1 mm) presented as punctate or linear low signal after implanted for 2 h. In (D) wet China rose (Length = 2 mm) presented as linear low signal after implanted for 2 h. Wet paulownia (Length = 2 mm) appeared as punctuate or linear low signal after implanted for 2 w in (E). And dry pine (Length = 2 mm) showed punctate or linear low signal after implanted for 4 w in (F).

water, anhydrous acetic acid and formaldehyde in the ratio of 10:7:2:1. The extracted eyebulb was immersed in the stationary liquid for 2-3 days and then in the anhydrous alcohol for 2-3 days. Paraffin embedding of the eyeball well was conducted by the professor from the Department of Basic Medicine, Zhengzhou University, which was observed by using light microscope after 5 μm serial section and HE staining. Presence of inflammation and kinds and amounts of inflammatory cells at different intervals were recorded.

Statistical analysis

SPSS16.0 (SPSS Inc., Chicago, IL, USA) was used to conduct statistical analysis (at the 5% significance level). Linear trend between the detection rate of foreign body of the same material and the change of length was performed by trend Chi-square test. One sample t test was introduced to compare the difference between the actual diameter and the observed diameter.

Results

Imageological characteristics of wooden IOFBs

After implantation for 2 h, 2 weeks and 4 weeks, the detected poplar, paulownia, pine, and China rose were all punctate or linear low signals on MRI (**Figure 1**). In this paper, the diagnostic complications on MRI included vitreous pneumatosis, eyebulb deformation and lens injury. And the vitreous pneumatosis appeared as circular or quasi-circular extreme low signals, around which high signals could be detected occasionally (**Figure 4A**). The eyebulb deformation presented as the eye-ring paramorphia and the lens injury as lens abnormalities (**Figure 4B**).

In this study, CT could not clearly detect the implanted IOFBs with length of 2 mm (**Figure 2**). Hence energy spectrum analysis was not furthered. Complications on CT included the vitreous pneumatosis (intravitreous circular or quasi-circular extreme low signals, **Figure 4C**), eyebulb deformation (the eye-ring paramorphia) and lens injury (lens abnormalities, **Figure 4D**).

For IOFBs punctured for 2 h, 2 weeks and 4 weeks, the ultrasonographic performance was detected as strong echo intensity (**Figure 3**). Complications on the ultrasonography involved

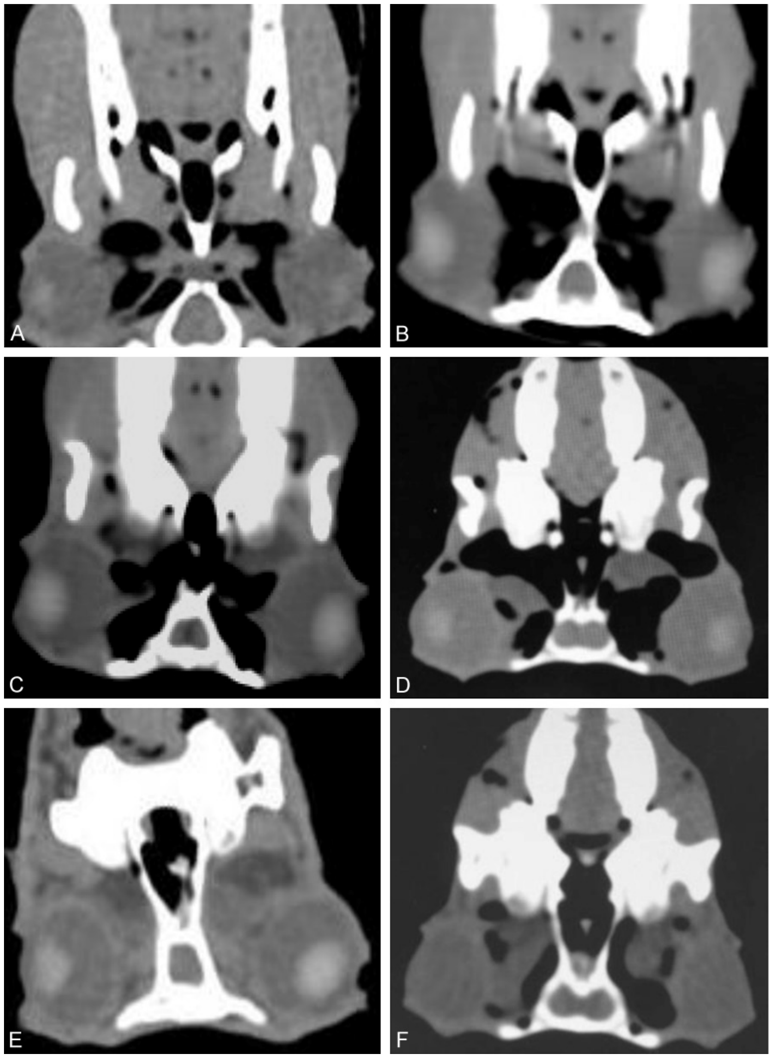

Figure 2. The characteristics of wooden IOFBs on transverse CT imaging. No abnormalities were detected for dry poplar (Length = 1 mm, 2 h) in (A), wet paulownia (Length = 2 mm, 2 h) in (B), dry pine (Length = 1 mm, 2 h) in (C), wet China rose (Length = 2 mm, 2 h) in (D), wet paulownia (Length = 2 mm, 2 w) in (E) and dry pine (Length = 2 mm, 4 w) in (F).

the vitreous opacity and lens injury, which presented as punctuate/linear/flocculent strong echo intensity (**Figure 4E**) and strong echo spot (**Figure 4F**), respectively.

Comparison of the detection rates of IOFBs and complications within the rabbit vitreous by MRI, CT and the ultrasonography

T_1WI could detect 8 out of 192 foreign bodies (4.1%), and 95 for T_2WI (49.5%) and 30 for PDWI (15.6%). The detection rate of MRI, represented by T_2WI, was compared with those of the CT and ultrasonography. Totally, MRI could detect 95 IOFBs with the detection rates of 49.5% and the ultrasonography 137 IOFBs with the detection rates of 71.4%, while CT could not detect all the IOFBs with the length of 2 mm. Results revealed that both the minimum detectable length of MRI and the ultrasonography towards dry IOFBs were 0.5 mm, and the detection rates increased with the length according to the Chi-squared test, indicating that length was the major factor affecting the sensitivity (Table S1). The minimum detectable length of MRI and the ultrasonography towards wet IOFBs were both 0.5 mm, and the detection rates increased with the length, suggesting that the length had main effects on the detection sensitivity (Table S2).

According to Table S3, detection rates of the ultrasonography towards the dry pine and Chine rose were significantly higher than those of MRI. No significant differences were found between the two methods towards the detection of dry poplar and paulownia as well as the wet IOFBs.

The detections of MRI and the ultrasonography were reckoned as the dependent variables and the lengths, materials and moisture states of the wooden IOFBs were evaluated as the explanatory variables. Then the binary logistic regression analysis was conducted and the forward remove method was adopted to incorporate the explanatory variables (Table S4). Results in Table S5 revealed that the length of IOFBs was the major factor affecting the detection rates of MRI, which was unassociated with the material and the moisture state. Logistic regression model containing all the three variables was applied to analyze detection rates of the ultrasonography. And no significance was found.

As shown in Table S6, insignificant differences were detected among the complications detection rates by the ultrasonography, CT and MRI

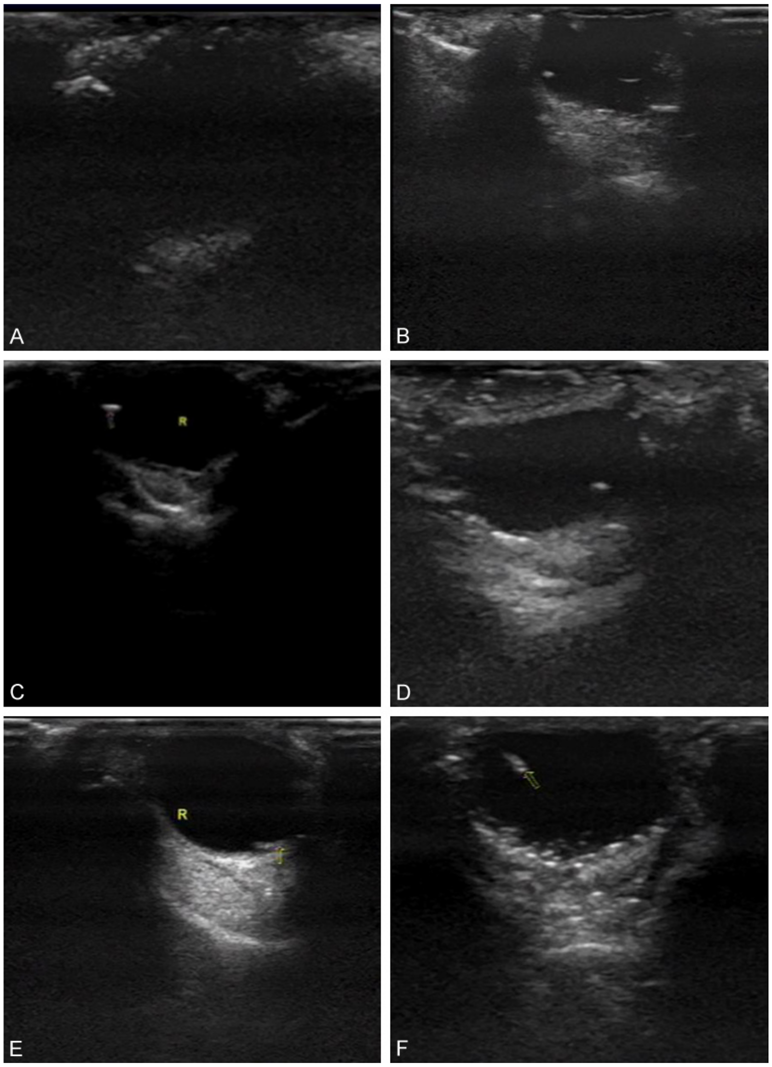

Figure 3. The characteristics of wooden IOFBs on the ultrasonography. Dry poplar (Length = 1 mm, 2 h) showed strong echo in (A). Wet paulownia (Length = 2 mm, 2 h) showed strong echo in (B). Dry pine (Length = 1 mm, 2 h) was strong echo in (C). Wet China rose (Length = 2 mm, 2 h) was strong echo in (D). Wet paulownia (Length = 2 mm, 2 w) was strong echo in (E). And dry pine (Length = 2 mm, 4 w) was strong echo in (F), accompanied with the multiple strong spots for the vitreous opacity.

towards IOFBs (Length = 2 mm) implanted for 2 h, 2 weeks and 4 weeks.

Comparison of the actual diameter and the observed diameter

MRI and the ultrasonography tended to overestimate the diameter and the measured diameters were significantly from the actual diameter (f = 0.2 mm). The observation of MRI (0.227±0.045 mm) was lower than that of the ultrasonography (0.250±0.050 mm), but close to the actual value. Due to the lowest sensitivity, the diameter observed by CT was deficient (Table S7).

Pathological results

HE stained eyebulb wells from 16 out of 48 rabbits implanted with IOFBs (Length of 2 mm) for 2 h indicated no inflammatory cells, and lymphocytes appeared in those 16 rabbits for 2 weeks, 9 with small amount (**Figure 5A**) and 7 with medium amount. Four weeks after the implantation, lymphocytes were generated in the other 16 rabbits, 1 with small amount, 7 with medium amount (**Figure 5B**) and 8 with large amount (**Figure 5C**). No inflammatory cells were examined in rabbits from the reference group.

Discussion

Detection difficulties of the wooden IOFBs increase with the unclear clinical history, normal diagnostic results and patients' neglect. With a lower incidence, wooden IOFBs might cause negligible and fast-healing wounds when entering the eye socket rapidly. Generally, the wooden IOFBs would fracture due to the high brittleness and leave no broken ends after the injury, which is one cause of missed diagnosis. IOFBs retention caused by the misdiagnosis could damage the eyebulb to a certain extent and induce serious complications [16]. Therefore it's of great significance for patients to receive timely and correct diagnosis and clinical removal to avoid infection and maintain visual function.

Cases of the intraocular non-magnetic low-density IOFBs detected by MRI but misdiagnosed by CT have been reported in recent researches [17]. Occasionally, wooden IOFBs are misdiagnosed as air by CT examination. With higher soft tissue resolution, MRI can distinctly reveal

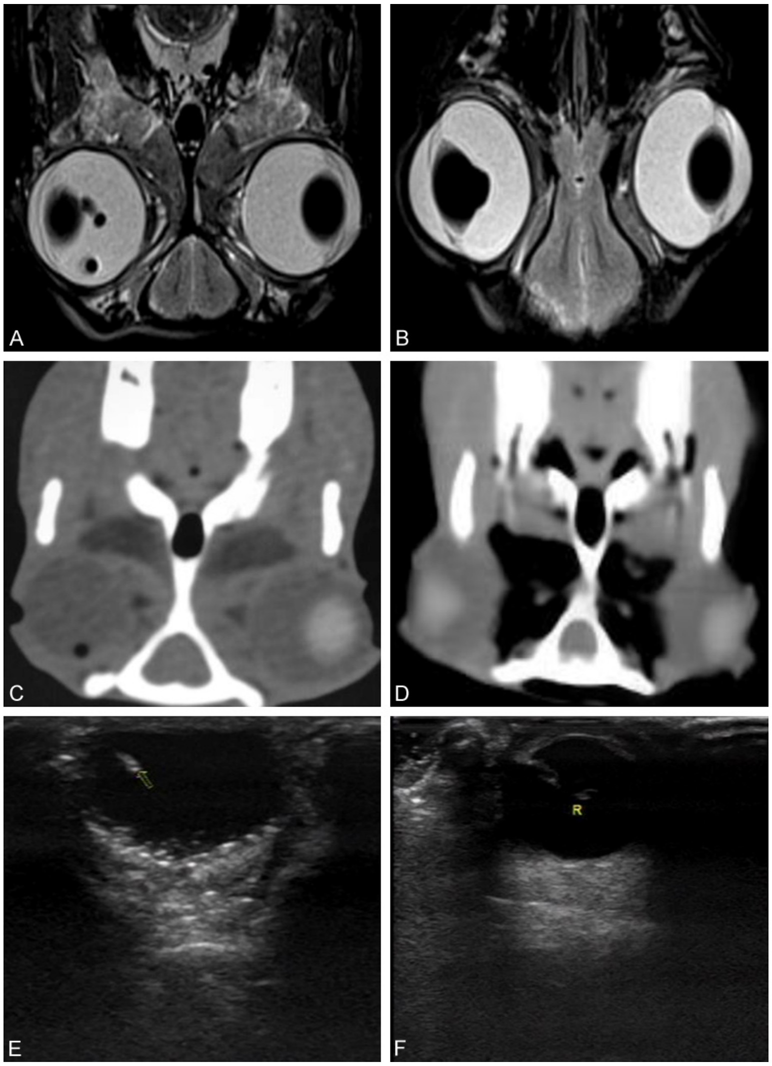

Figure 4. The characteristic complications of the rabbit vitreous implanted with wooden IOFBs. In (A) wet pine (Length = 0.5 mm, 2 h) presented circular extreme low signals on transverse MRI imaging and high signals peripherally combined with the vitreous pneumatosis. In (B) dry paulownia (Length = 1 mm, 2 h) induced the lens paramorphia on transverse MRI imaging. In (C) wet pine (Length = 0.5 mm, 2 h) caused the vitreous pneumatosis with circular gas density on transverse CT imaging. In (D) dry paulownia (Length = 1 mm, 2 h) caused the lens paramorphia and deformation on transverse CT imaging. In (E) was the ultrasonic imaging for wet pine (Length = 0.5 mm, 2 h) with the vitreous opacity. In (F) the lens injury presented stronger echo intensity caused by dry paulownia (Length = 1 mm, 2 h) on the ultrasonic imaging.

the number and intraocular location of wooden IOFBs and exactly identify lesions within the normal ocular structures, indicating the common complications and anatomical structures surrounding the IOFBs [18, 19]. The ultrasonography is unconstrained by the properties of IOFBs, and the detection results are associated with the size and the reflection interface, showing high sensitivity against the IOFBs. Based on the abnormal echo from different acoustical surfaces, this technology can locate the IOFBs accurately and observe the corresponding complications, e.g. the phacoscotasmus, vitreous opacity and retinal detachment. Above all, MRI and the ultrasonography are effective in detecting and locating the non-magnetic IOFBs, especially for the wooden IOFBs infeasible for CT examination.

CT examination can clearly present IOFBs of high density with intuitionistic images and reveal positional relationship between the IOFBs and the ocular well. Results were diverse on the CT detection of wooden IOFBs [20-23]. Krimmel et al. reported that wooden IOFBs showed high density signals on CT after intraocular retention for several months [24]. Lee et al. found that CT could only detect calcified wooden IOFBs [25]. In our study, CT examination could not identify 48 wooden IOFBs (Length = 2 mm) implanted in the rabbit right vitreous for 2 h, 2 w and 4 w. Hence the spectrum analysis wasn't further performed. Appropriate window width and window level were unavailable for the tiny IOFBs in this paper to distinguish them from the normal vitreous tissue, which should be advanced by adjusting the diameter of IOFBs. CT value of the vitreous was (-94.4±9.9) Hu, similar to that of wooden IOFBs (-145~63.8 Hu in this paper), which was adverse to the IOFBs display. Reconstruction interval and layer spacing would affect the IOFBs development. And misdiagnosis would occur due to the invisibility and/or inauthentic density of IOFBs positioning squarely between the two layers. Punctiform or streak artifacts generated from the instrument would also

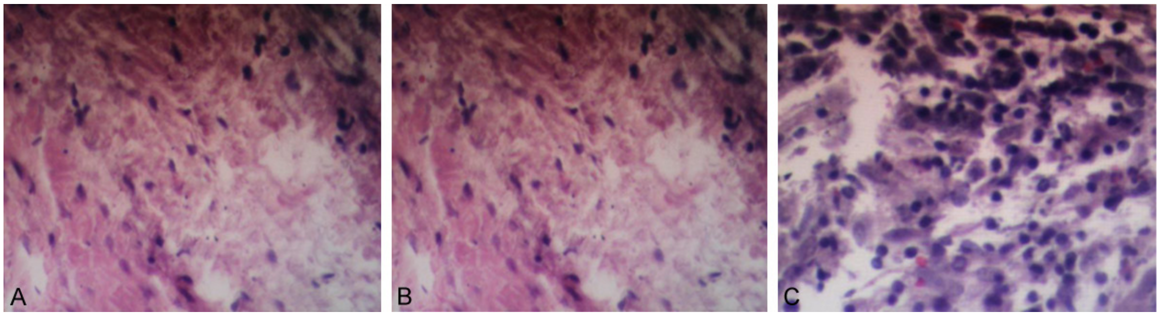

Figure 5. The microscopic images for the pathological examination (HE staining, ×400). In (A) a few circular and quasi-circular hyperchromatic lymphocytes appeared in the vitreous implanted with wooden IOFBs for 2 w. And medium circular and quasi-circular hyperchromatic lymphocytes could be detected in pathological section of ocular wall from the vitreous implanted with IOFBs for 2 w in (B). Large amounts of circular and quasi-circular hyperchromatic lymphocytes could be investigated in pathological section of ocular wall from the vitreous implanted with IOFBs for 4 w in (C).

affect the IOFBs detection [26]. Additionally, partial volume effects could also impact the distinct presence of foreign bodies [27].

The ultrasonography is characterized by the good repeatability, high resolution and real-time imaging, which is effective in the detection of low-density foreign bodies. Echo intensity of the IOFBs is dependent on the difference of acoustic impedance between the IOFBs and the peripheral tissue. The echo intensity of intraocular foreign body is enhanced considerately due to the higher acoustic impedance difference [28]. In general, the acoustic impedance difference between non-metallic foreign bodies (e.g. wooden IOFBs) and the vitreous was smaller and the ultrasonic echo between the two surfaces was relatively weaker, which presents as the strong echo intensity or light strip within the liquid anechoic area of the vitreous, accompanied with posterior shadowing or not. In this study, the ultrasonography detected 137 from the 192 IOFBs and possessed the maximal detection rate (71.4%). The observed diameter was higher than the actual diameter (f = 0.2 mm). Signals of wooden IOFBs presented as strong echo band on the front edge and absence of echo on the back due to the ultrasonic attenuation. IOFBs in this research were all punctured within the vitreous and showed strong echo intensity. After reducing the gain, 48 IOFBs with length of 0.2 mm were still undetected, which might be related with the ultrasonic resolution [29].

Magnetic induction is the property of materials affecting the local magnetic line of force in the magnetic field. Due to protons absence, the wooden IOFBs present as the signal loss on MRI. We detected that the vitreous showed high signals on T_2WI and the wooden IOFBs appeared as the punctuate or linear low signals with shapes dependent on the puncturing direction and the scan section, the distinct contrast between which were conducive to the IOFBs display [30]. Totally, 95 IOFBs could be detected on T_2WI (Detection rate = 49.5%). IOFBs with the length of 2 mm were all identified, while those with 1 mm or 0.5 mm were partially figured out. The detectable length might be related with the partial volume effect and the resolution of T_2WI. The measured diameter was close to the actual diameter, probably involved with the high contrast between the IOFBs and the vitreous on T_2WI.

The minimum lengths of four wooden IOFBs on MRI and the ultrasonography were all 0.5 mm. As indicated in the trend Chi-square test, the detection rates of the two methods increased with the length. The detection sensitivity of CT examination was the lowest, even for those 2 mm IOFBs. Consequently, the length was the major factor affecting the detection rates. And the other two factors (i.e. the material and the moisture state) had no significant effect on the detection results, which had been confirmed in the logistic recession analysis.

Common complications of the IOFBs include the vitreous hemorrhage, pneumatosis and lens opacity. And larger ones would cause the eyebulb deformation. On MRI and CT examination, the detected complications contained the lens opacity, the eyebulb deformation and the lens injuries. On the ultrasonography, those involved the vitreous opacity and the lens injuries. Due to the tiny size in our study, the observed eyebulb deformation might be relevant with the vitreous overflow during the puncture, the vitreous hemorrhage caused by entrained air during the implantation and the lens injury induced by damaging the lens when lowering the wooden IOFBs into the vitreous or the changes of lens due to the IOFBs retention. The vitreous hemorrhage on T_2WI showed the punctuate extremely-low signals and visible high signals peripherally, induced by the chemical displacement and interfacial artifacts, which presented as circular gas density shadow. Signals of the eyebulb deformation were paramorphia of the eye ring on the T_2WI and CT. The lens paramorphia as the strong echo on the ultrasonography indicated the lens injury. The vitreous opacity was just detected by the ultrasonography, appearing as the punctiform, linear and flocculent strong echo. Differences among the detected complications by MRI, CT and the ultrasonography were insignificant.

Inflammatory cells existed only within the ocular well around the IOFBs and increased with the retention. Länsman et al. studied the intraocular implantation of absorbable plant tissue, revealing that the pathologic changes were confined to the implanted sites and fibrous tissue and inflammatory cells increased over time [31]. Diverse pathological changes were produced along with the intraocular retention. The histocompatibility of wooden IOFBs was good and lesions at early phase were less severe. Results indicated that inflammation on the ocular well around the implantation sites were deteriorated with the IOFBs retention, suggesting the importance of timely diagnosis and correct removal of IOFBs.

Conclusions

MRI and the ultrasonography are the optimal methods for detecting the wooden IOFBs, and MRI examination could provide abundant information for clinical diagnosis and treatment. The length was the major factor affecting the wooden IOFBs (f = 0.2 mm) detection by MRI. The ultrasonography could accurately identify the IOFBs and the complications. CT examination was infeasible to detect wooden IOFBs but this technology could reveal the intraocular complications. Retention of wooden IOFBs would induce the inflammatory changes. Combined with the characteristics of imageological examination, the clinician should select appropriate detecting methods in terms of the trauma degree and possible of the IOFBs.

Acknowledgements

The paper was funded by the project “The imaging contrast empirical study of the intraocular foreign body” granted by the Basic and advanced technology research project, Department of Science and Technology of Henan Province (No. 122300410364). The authors expressed thanks to crews from the Department of MRI in the First Affiliated Hospital of Zhengzhou University for providing determination and valuable discussion.

Disclosure of conflict of interest

None.

Address correspondence to: Jingliang Cheng, Department of MRI, The First Affiliated Hospital of Zhengzhou University, 1 Jianshe East Road, Zhengzhou 450052, Henan Province, P. R. China. Tel: +86 371 66913672; Fax: +86 371 66913672; E-mail: chengjingliang126@126.com

References

[1] Romaniuk VM. Ocular trauma and other catastrophes. Emerg Med Clin North Am 2013; 31: 399-411.
[2] Wong TY, Seet MB, Ang CL. Eye injuries in twentieth century warfare: a historical perspective. Surv Ophthalmol 1997; 41: 433-459.
[3] Zhang Y, Zhang MN, Jiang CH, Qiu HY. Intraocular foreign bodies in china: clinical characteristics, prognostic factors, and visual outcomes in 1421 eyes. Am J Ophthalmol 2011; 152: 66-73, e1.
[4] Griffiths ML, Lee GA. Retained intraocular foreign body. Clin Exp Optom 2004; 87: 34-36.
[5] Baumeister M, Kuhli-Hattenbach C, Luchtenberg M. Corneal ulcer caused by a wooden foreign body in the upper eyelid 6 months after minor injury. Ophthalmologica 2006; 220: 397-399.
[6] Covert DJ, Henry CR, Sheth BP. Well-tolerated intracorneal wood foreign body of 40-year duration. Cornea 2009; 28: 597-598.
[7] Rubsamen PE, Cousins SW, Winward KE, Byrne SF. Diagnostic ultrasound and pars plana vitrectomy in penetrating ocular trauma. Ophthalmology 1994; 101: 809-814.

[8] Pinto A, Brunese L, Daniele S, Faggian A, Guarnieri G, Muto M, Romano L. Role of computed tomography in the assessment of intraorbital foreign bodies. Semin Ultrasound CT MR 2012; 33: 392-395.
[9] Tonini M, Krainik A, Bessou P, Lefournier V, Boubagra K, Chiquet C, Le Bas JF. How helical CT helps the surgeon in oculo-orbital trauma. J Neuroradiol 2009; 36: 185-198.
[10] Dass AB, Ferrone PJ, Chu YR, Esposito M, Gray L. Sensitivity of spiral computed tomography scanning for detecting intraocular foreign bodies. Ophthalmology 2001; 108: 2326-2328.
[11] Bailey W, Robinson L. Screening for intra-orbital metallic foreign bodies prior to MRI: review of the evidence. Radiography 2007; 13: 72-80.
[12] Lin HC, Wang HZ, Lai YH. Occult plastic intravitreal foreign body retained for 30 years: a case report. Kaohsiung J Med Sci 2006; 22: 529-533.
[13] Green BF, Kraft SP, Carter KD, Buncic JR, Nerad JA, Armstrong D. Intraorbital wood: detection by magnetic resonance imaging. Ophthalmology 1990; 97: 608-611.
[14] Berkowitz BA, McDonald C, Ito Y, Tofts PS, Latif Z, Gross J. Measuring the human retinal oxygenation response to a hyperoxic challenge using MRI: eliminating blinking artifacts and demonstrating proof of concept. Magn Reson Med 2001; 46: 412-416.
[15] Yang Y, Cheng J, Wang J, Zhang Y, Li HL. Characteristic analysis on susceptibility weighted imaging of intravitreous foreign body of autologous eyelashes in rabbits. Chin J Traumatol 2010; 13: 304-307.
[16] Bhagat N, Nagori S, Zarbin M. Post-traumatic infectious endophthalmitis. Surv Ophthalmol 2011; 56: 214-251.
[17] Lagalla R, Manfre L, Caronia A, Bencivinni F, Duranti C, Ponte F. Plain film, CT and MRI sensibility in the evaluation of intraorbital foreign bodies in an in vitro model of the orbit and in pig eyes. Eur Radiol 2000; 10: 1338-1341.
[18] Chazen JL, Lantos J, Gupta A, Lelli GJ Jr, Phillips CD. Orbital soft-tissue trauma. Neuroimaging Clin N Am 2014; 24: 425-437.
[19] Ho VT, McGuckin JF, Smergel EM. Intraorbital wooden foreign body: CT and MR appearance. Am J Neuroradiol 1996; 17: 134-136.
[20] John SS, Rehman TA, John D, Raju RS. Missed diagnosis of a wooden intra-orbital foreign body. Indian J Ophthalmol 2008; 56: 322.
[21] Lakshmanan A, Bala S, Evans Belfer KF. Intraorbital organic foreign body-a diagnostic challenge. Orbit 2008; 27: 131-133.
[22] Paul AM, Grundmann T. Intraorbital wooden foreign body undetected on CT. HNO 2010; 58: 1237-1240.
[23] Uchino A, Kato A, Takase Y, Kudo S. Intraorbital wooden and bamboo foreign bodies: CT. Neuroradiology 1997; 39: 213-215.
[24] Krimmel M, Cornelius CP, Stojadinovic S, Hoffmann J, Reinert S. Wooden foreign bodies in facial injury: a radiological pitfall. Int J Oral Maxillofac Surg 2001; 30: 445-447.
[25] Lee JS, Lee JE, Oum BS, Cha SH. Orbitocranial injury caused by wood. Korean J Ophathalmol 1999; 13: 128-132.
[26] Arey ML, Mootha VV, Whittemore AR, Chason DP, Blomquist PH. Computed tomography in the diagnosis of occult open-globe injuries. Ophthalmology 2007; 114: 1448-1452.
[27] Czyz CN, Kondapalli SS, Mazzuca DE Jr, Allen SH, Cahill KV. Variant of Giant Fornix Syndrome Masquerading as Intraocular Free Air on Computed Tomography. J Emerg Med 2013; 44: e311-e313.
[28] Sawyer MN. Ultrasound imaging of penetrating ocular trauma. J Emerg Med 2009; 36: 181-182.
[29] Leo M, Carmody K. Sonography assessment of acute ocular pathology. Ultrasound Clin 2011; 6: 227-234.
[30] Moisseiev E, Last D, Goez D, Barak A, Mardor Y. Magnetic resonance imaging and computed tomography for the detection and characterization of nonmetallic intraocular foreign bodies. Retina 2015; 35: 82-94.
[31] Länsman S, Pääkkö P, Ryhänen J, Hirvelä H, Kellomäki M, Ellä V, Törmälä P, Waris T, Ashammakhi NA. Histologic analysis of bioabsorbable scleral buckling implants: an experimental study on rabbits. Retina 2005; 25: 1032-1038.

Table S1. Comparison between detection rates by MRI, CT and the ultrasonography

Materials	*Length/mm*	*MRI (T_2WI)*		*CT*		Ultrasonography	
		ND	D	ND	D	ND	D
Poplar	0.2	6	0	-	-	6	0
	0.5	3	3	-	-	1	5
	1.0	4	2	-	-	0	6
	2.0	0	6	6	0	0	6
	χ^2 (P)	9.769 (0.002)				9.439 (0.002)	
Paulownia	0.2	6	0	-	-	6	0
	0.5	3	3	-	-	1	5
	1.0	3	3	-	-	0	6
	2.0	0	6	6	0	0	6
	χ^2 (P)	9.976 (0.002)				9.439 (0.002)	
Pine	0.2	6	0	-	-	6	0
	0.5	3	3	-	-	0	6
	1.0	3	3	-	-	0	6
	2.0	0	6	6	0	0	6
	χ^2 (P)	9.976 (0.002)				8.631 (0.002)	
China rose	0.2	6	0	-	-	6	0
	0.5	3	3	-	-	0	6
	1.0	3	3	-	-	0	6
	2.0	0	6	6	0	0	6
	χ^2 (P)	9.976 (0.002)				8.631 (0.002)	

ND: Non-detected; D: Detected. The minimum detectable lengths of MRI and the ultrasonography were both 0.5 mm. As revealed by the trend Chi-square test, the detection rates increased with the lengths. The detection sensitivity of CT examination was the lowest, and this technology couldn't even detect the IOFBs with the length of 2 mm.

Table S2. Comparison between detection rates by MRI, CT and the ultrasonogaphy

Materials	*Length/ mm*	*MRI (T_2WI)*		*CT*		Ultrasonography	
		ND	D	ND	D	ND	D
Poplar	0.2	6	0	-	-	6	0
	0.5	3	3	-	-	1	5
	1.0	3	3	-	-	0	6
	2.0	0	6	6	0	0	6
	χ^2 (P)	9.769 (0.002)				9.439 (0.002)	
Paulownia	0.2	6	0	-	-	6	0
	0.5	3	3	-	-	2	4
	1.0	3	3	-	-	0	6
	2.0	0	6	6	0	0	6
	χ^2 (P)	9.976 (0.002)				14.407 (0.001)	
Pine	0.2	6	0	-	-	6	0
	0.5	3	3	-	-	1	5
	1.0	3	3	-	-	0	6
	2.0	0	6	6	0	0	6
	χ^2 (P)	9.976 (0.002)				9.439 (0.002)	
China rose	0.2	6	0	-	-	6	0
	0.5	4	2	-	-	1	5
	1.0	2	4	-	-	0	6
	2.0	0	6	6	0	0	6
	χ^2 (P)	11.909 (0.001)				9.439 (0.002)	

ND: Non-detected; D: Detected. The minimum detectable lengths of MRI and the ultrasonography were both 0.5 mm. The detection rates increased with the length. CT examination couldn't detect all the IOFBs.

Table S3. Comparison between detection rates by MRI and the ultrasonograpgy

Materials	*MRI (T_2WI)*	*Ultrasonography (For dry IOFBs)*		*Ultrasonography (For wet IOFBs)*	
		ND	D	ND	D
Poplar	ND	6	7	7	5
	D	1	10	0	12
	χ^2 (P)	3.125 (0.077)		3.200 (0.074)	
Paulownia	ND	6	6	7	5
	D	1	11	1	11
	χ^2 (P)	2.286 (0.131)		1.500 (0.221)	
Pine	ND	6	6	6	6
	D	0	12	1	11
	χ^2 (P)	4.167 (0.041)		2.286 (0.131)	
China rose	ND	6	6	6	6
	D	0	12	1	11
	χ^2 (P)	4.167 (0.041)		2.286 (0.131)	

Significant differences were identified for the detection of dry pine and China rose (*P*<0.05). Differences between the detection rates for wet wooden IOFBs were insignificant (*P*>0.05).

Table S4. Variable declaration for the logistic regressions

	Variable declaration	*Assignment*
Dependent variables	Detection by MRI (T_2WI)	0 = ND; 1 = D
	Detection by the ultrasonography	0 = ND; 1 = D
Explanatory variables	Materials*	1 = Poplar; 2 = Paulownia; 3 = Pine; 4 = China rose
	Lengths	Original values
	Moisture states	1 = Dry IOFBs; 2 = Wet IOFBs

*Variables were integrated into the model as the dummy variables, Reference = 1; ND: Non-detected; D: Detected.

Table S5. Results of factor analysis for MRI (T_2WI) detection, the MRI detection was unaffected by the material and the moisture state

Explanatory variable	*β*	*Wald*	*P*	*OR*	*95.0% CI*
Length	3.254	45.523	<0.001	25.881	10.058-66.595
Constant term	-2.705	46.369	<0.001	0.067	

Table S6. Comparison of the detected complications by the three methods, differences between the three methods for detecting after the wooden IOFBs implanted for 2 h, 2 w and 4 w

Retention time	*Moisture states*	*Materials*	*MRI (T_2WI)*			*CT*			*Ultrasonography*		
			ND	D	P	ND	D	P	ND	D	P
2 h	Dry	Poplar	4	2	>0.999	4	2	>0.999	4	2	>0.999
		Paulownia	4	2		4	2		5	1	
		Pine	5	1		5	1		5	1	
		China rose	4	2		4	2		5	1	
	Wet	Poplar	4	2	>0.999	5	1	>0.999	3	3	>0.999
		Paulownia	4	2		4	2		5	1	
		Pine	4	2		4	2		5	1	
		China rose	4	2		4	2		4	2	
2 w	Dry	Poplar	2	2	>0.999	2	2	>0.999	2	2	>0.999
		Paulownia	3	1		3	1		3	1	
		Pine	3	1		3	1		3	1	
		China rose	3	1		3	1		3	1	
	Wet	Poplar	3	1	>0.999	4	0	>0.999	2	2	>0.999
		Paulownia	2	2		3	1		3	1	
		Pine	4	0		3	1		3	1	
		China rose	3	1		3	1		2	2	
4 w	Dry	Poplar	1	1	>0.999	1	1	>0.999	0	2	>0.999
		Paulownia	1	1		1	1		1	1	
		Pine	1	1		1	1		1	1	
		China rose	2	0		2	0		1	1	
	Wet	Poplar	2	0	>0.999	2	0	>0.999	1	1	>0.999
		Paulownia	1	1		1	1		1	1	
		Pine	1	1		1	1		0	2	
		China rose	2	0		2	0		1	1	

Table S7. Comparison of the observed diameter and the actual diameter (Φ = 0.2 mm)

Detection methods	*Observed diameter (Means ± S) mm*	*T value*	*P value*
MRI (T_2WI)	0.227±0.045	5.95	<0.001
CT	-	-	-
Ultrasonography	0.250±0.050	11.49	<0.001

MRI and the ultrasonography tended to overestimate the diameter (P<0.05). The measurement by MRI was close to the actual diameter. And the CT observation was missing due to the lowest sensitivity.